Appl. Phys. B 74 [Suppl.], S193–S200 (2002)
DOI: 10.1007/s00340-002-0872-1

Applied Physics B
Lasers and Optics

M. GUINA✉
N. XIANG
O.G. OKHOTNIKOV

Stretched-pulse fiber lasers based on semiconductor saturable absorbers

Optoelectronics Research Centre, Tampere University of Technology, P.O. Box 692, 33101, Tampere, Finland

Received: 14 September 2001 / Revised version: 7 January 2002
Published online: 20 June 2002 •

ABSTRACT Stretched-pulse mode-locked erbium-doped fiber lasers based on monolithically grown InGaAsP/InP semiconductor saturable absorber mirrors are described. The saturable absorbers are used to initiate the mode locking, to stabilize the pulse train and to control the cavity dispersion. We obtained reliable operation at the fundamental repetition rate with 1.3 nJ of pulse energy, limited by the maximum available pump power of 175 mW. The amplitude fluctuation was estimated to be less than 1.6×10^{-3}. 135-fs transform-limited pulses were obtained after compression in standard telecommunication fiber. The performance of the stretched-pulse mode-locked fiber laser with near-resonant semiconductor saturable absorber has been studied. A semiconductor dispersive saturable absorber mirror was used for intracavity chirp compensation in the stretched-pulse fiber laser. With the semiconductor mirror combining both negative group-velocity dispersion and saturable absorption, we have demonstrated the production of high-power chirp-free pulses directly from stretched-pulse laser.

PACS 42.55.Wd; 42.60.Fc

1 Introduction

The stretched-pulse mode-locked fiber laser presents an attractive design for efficient pulse energy extraction from fiber amplifiers [1, 2]. It can deliver single-pulse energies that are three orders of magnitude higher than those of a soliton laser [3]. Although the tendency for multiple-pulse operation is reduced in the stretched-pulse laser by limiting non-linear propagation to fiber of normal dispersion and avoiding soliton effects, at higher powers multiple-pulse generation within the cavity has been observed, thus decreasing the fundamental pulse energy [3]. Mode-locked lasers based on the stretched-pulse principle routinely exploit the additive-pulse mode-locking (APM) mechanism as a fast saturable absorber. Multiple-pulse behavior at high pump powers is caused by saturation of the APM [4]. With properly biased APM, the fundamental pulse train could be obtained, however at such bias points self-starting operation is unlikely. Self-starting operation becomes even more problematic with linear laser geometry due to standing wave effects and spurious reflections. Active mode locking can be used as a starting mechanism in a stretched-pulse laser, however, it requires an extra modulator for assistance with the pulse start-up. After mode locking is initiated by turning on the modulator, the modulator is turned off [1].

Semiconductor saturable absorber mirrors (SESAMs) have been used successfully to initiate and to sustain mode-locking in a wide range of solid-state and fiber lasers [5]. The main advantage of the SESAM is the possibility of controlling important parameters such as the absorption recovery time, saturation fluence and insertion loss through the device design, growth conditions and heavy ion implantation. Exploiting the SESAM as a cavity mirror in the fiber laser results in compact size, environmentally stable and simple ultrashort-pulse lasers that can cover wide wavelength range and generate optical pulses with durations from picoseconds to femtoseconds.

As has been pointed out, without pulse shaping by soliton formation, an absorber with a response as fast as possible is always desirable [5]. However, in general, lasers mode-locked by fast saturable absorbers have an intrinsic problem with self-starting from a continuous-wave operation due to insufficient pulse shaping for long pulses [2]. Mode locking of the laser can be easily initiated and stabilized by the saturation dynamics of the slow absorber. However, the pulses develop a trailing wing due to the absorber recovering slowly [5].

In this paper we demonstrate another approach, based on a stretched-pulsed fiber laser with two SESAMs – one slow and one fast. We show that fundamental stretched-pulse mode locking can be started and stabilized by a slow absorber, while a fast absorber can preserve the pulse quality. We demonstrate a fiber laser with SESAM that combines both saturable absorption and dispersion compensation. A dispersive saturable absorber mirror (D-SAM) was used for changing the average cavity dispersion and forcing the laser to operate in the stretched-pulse mode-locking regime or the soliton-assisted regime. D-SAM with negative group-velocity dispersion (GVD) was used for intracavity chirp compensation, giving rise to high-energy transform-limited pulses without the need for external pulse compression. D-SAM with positive GVD was optimized for the stretched-pulse regime, thus avoiding the use of dispersion-compensating fiber and, therefore, reducing the non-linear effects in the laser cavity.

✉ Fax: +358-3-3115-3400, E-mail: Mircea.Guina@orc.tut.fi

2 High-energy pulse generation in a self-starting stretched-pulse fiber laser mode-locked and stabilized with slow and fast semiconductor saturable absorbers

The stretched-pulse laser includes segments of positive-dispersion fiber and negative-dispersion fiber, with an overall dispersion that is slightly positive [1–3]. The experimental set-up and the dispersion map for a stretched-pulse mode-locked laser with two absorbers are illustrated in Fig. 1. The fiber cavity includes 1.3 m of erbium-doped fiber and 40 cm of dispersion compensating fiber. The erbium-doped fiber had an unpumped loss of 38 dB/m at 1.535 μm, a core diameter of 6.2 μm, a numerical aperture NA = 0.23 and normal group-velocity dispersion (GVD) of $+0.01\,\mathrm{ps}^2/\mathrm{m}$ at 1.56 μm. The dispersion-compensating fiber had a normal GVD of $+0.16\,\mathrm{ps}^2/\mathrm{m}$ at 1.56 μm. The 50% output coupler was made from Corning SMF28 fiber with a GVD of $-0.023\,\mathrm{ps}^2/\mathrm{m}$ at 1.56 μm. The cavity also contained a Corning Flexcor 1060 fiber with a GVD of $-0.007\,\mathrm{ps}^2/\mathrm{m}$, which formed the 980/1550 nm wavelength-selective coupler used to launch the pump. The round-trip dispersion of the cavity was estimated from measurements to be $+0.029\,\mathrm{ps}^2$ in the normal dispersion regime. The fiber ends were angle-polished to eliminate the influence of Fresnel reflection. AR-coated aspheric lenses with focal lengths of 2.0 mm were used to focus the beam onto the absorbers. The laser was pumped with a single-mode grating-stabilized laser diode, which provided a power of 175 mW at 980 nm. The laser set-up gave a fundamental repetition rate of approximately 18.8 MHz.

The SESAM was grown by all-solid-source molecular-beam epitaxy on a *S*-doped *n*-type InP (100) substrate. As a semiconductor mirror, we used a broadband (≈ 120 nm), high-reflectivity Burstein–Moss shifted Bragg reflector composed of 19.5 pairs of quarter-wave n^+-$Ga_{0.47}In_{0.53}As$/InP layers [6]. The saturable absorber consisted of an InP spacer layer, four 7-nm-thick GaInAsP quantum wells separated by 8-nm InP barriers, and an 80-nm-thick InP cap. To decrease the absorption recovery time of the device used as a fast SESAM, this sample was post-growth irradiated with 30-MeV nickel ions at a dose of $10^{12}\,\mathrm{cm}^{-2}$. Although the recovery time of the absorbers was not measured directly, the speed of the absorbers was estimated using results presented in [7]. For the same parameters of Ni^+ implantation, we could estimate that the non-linear recovery time was reduced from approximately 1 ns for the non-implanted sample down to approximately 2–4 ps for the Ni^+-implanted sample. The saturable absorber was designed to work in anti-resonance over the full band of the semiconductor mirror [8].

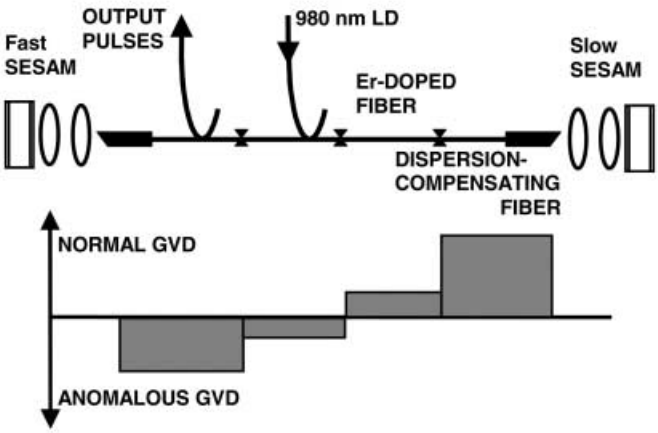

FIGURE 1 Set-up of the stretched pulse fiber laser with two absorbers and illustrative sketch of the dispersion map of the cavity

To study the dynamics of the stretched-pulse laser mode locked by fast and slow absorbers, attempts were made to avoid the polarization-APM mechanism by minimizing the polarization sensitivity of the cavity elements. Thus, the pulse was dominantly shaped by the saturable absorbers. In the linear cavity configuration, the high-energy pulse stretched in the normal dispersion fiber was focused onto the slow SESAM, while the pulse compressed in the negative dispersion fiber, with the energy reduced by outcoupling, was directed to the fast absorber. The main idea behind this laser configuration was that the losses experienced by the wide-width stretched pulses were much less in the case of the slow absorber than with the fast saturable absorber. Moreover, mode locking of the laser could be easily initiated by the saturation dynamics of the slow absorber, in contrast to the fast absorbers, which had insufficient pulse-shaping capability for long pulses. We found that optimum operation in our stretched-pulse laser in terms of pulse quality and discrimination against pulse break up could be obtained with oversaturated fast absorber and with weaker saturation of slow absorber. Since pulse break-up is favored if the absorber is highly saturated [5], an antiresonant Fabry–Perot design was used with additional dielectric coating as a top reflector. A dielectric coating providing a reflectivity of 60% was applied on top of the slow SESAM to increase the saturation fluence and to prevent pulse break-up. Additionally, this reduced the risk of optical damage to the SESAM caused by high-energy stretched pulses hitting the slow absorber. The top reflectivity for the uncoated fast absorber was about 27%. The saturation fluence was estimated from measurements to be about $E_{\mathrm{sat}}^{\mathrm{slow}} \approx 120\,\mu\mathrm{J/cm}^2$ for the slow absorber and about $E_{\mathrm{sat}}^{\mathrm{fast}} \approx 70\,\mu\mathrm{J/cm}^2$ for the fast SESAM. For the proposed laser configuration, the fluence on the absorbers could be adjusted independently by changing the focusing condition. As a result, highly reliable and self-starting mode locking to a single pulse per round trip was achieved at 50 mW of pump power. Figure 2a shows a typical pulse spectrum with a square shape, supporting the concept of the formation of a chirped-pulse structure. Autocorrelation of the pulse is shown in Fig. 2b. With a non-optimized output coupling, a pulse energy of 1.3 nJ was obtained with the pump power under 175 mW. With optimized output coupling, higher pulse energy can be produced for a given pump level [2].

To estimate the amplitude noise, we have measured the rf power spectrum near the fundamental frequency component. Without phase fluctuation, the amplitude fluctuation is given by: $\Delta A/A = [(P_{\mathrm{a}}\Delta f_{\mathrm{a}}) / (P_{\mathrm{s}}\Delta f_{\mathrm{res}})]^{1/2}$ [9], where ΔA is the root-mean-square deviation from the average pulse amplitude A; P_{s} is the peak power of the fundamental harmonic and P_{a} is the peak power in the amplitude noise band; Δf_{a}

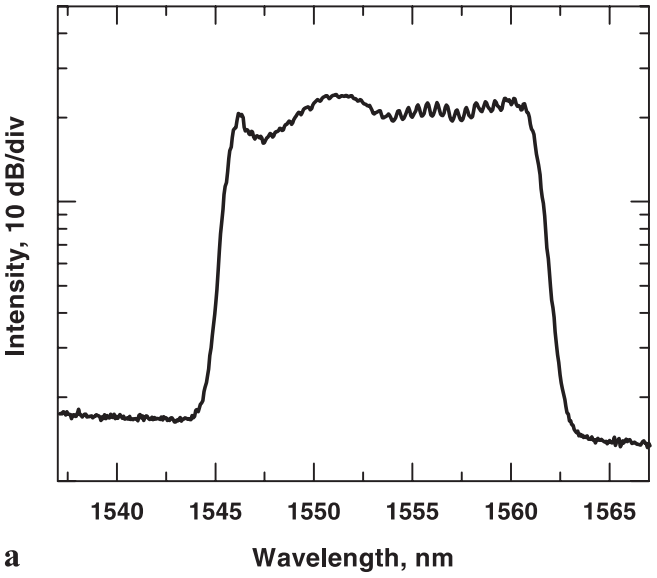

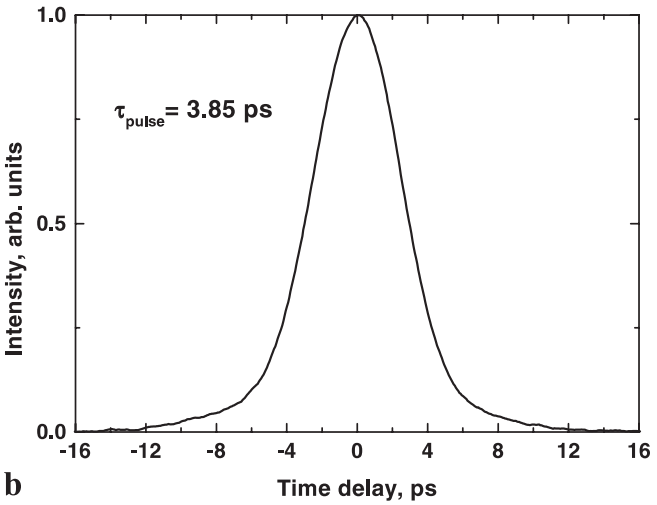

FIGURE 2 **a** Typical spectrum with $\Delta\lambda = 16.2$ nm; and **b** autocorrelation trace of a pulse from a stretched-pulse laser with two absorbers

is the FWHM bandwidth of the amplitude noise band and Δf_{res} is the resolution bandwidth of the microwave spectrum analyzer. The rf spectrum around the fundamental harmonic showed that the noise amplitude was more than 75 dB lower than the fundamental frequency peak. With $\Delta f_{\text{a}} = 80$ KHz and $\Delta f_{\text{res}} = 1$ kHz, the amplitude fluctuation was estimated to be $\Delta A/A \approx 1.6 \times 10^{-3}$.

At the laser output, we used a dispersive delay line to accomplish the chirp compensation. A plot of pulse width versus dispersion in the delay line is shown in Fig. 3 for output pulses with a bandwidth of 22 nm. For a dispersion of approximately -0.01 ps^2 we obtained a minimum pulse width of 135 fs. The time–bandwidth product was reduced to 0.38. This shows that the de-chirped pulses were of high quality, thus confirming the high linearity of chirp produced in the cavity section with normal dispersion.

To highlight the role of each absorber, their contribution was studied separately by replacing one of the absorbers with a high-reflectivity dielectric mirror. It was found that the slow SESAM ensured reliable self-starting of the fundamental mode-locked operation with no indication of multiple pulse break-up up to highest pump power available. However, the autocorrelation had large wings that contained a considerable fraction of the energy due to a long, low-loss window following the pulse. Alternatively, with fast absorber, mode locking was difficult to initiate. The self-starting required initiation by translating the saturable absorber mirror to perturb the cavity. Once the mode locking with pedestal-free pulses was established, the pulse broke up into multiple pulses with increase in pump power, thus limiting the pulse energy.

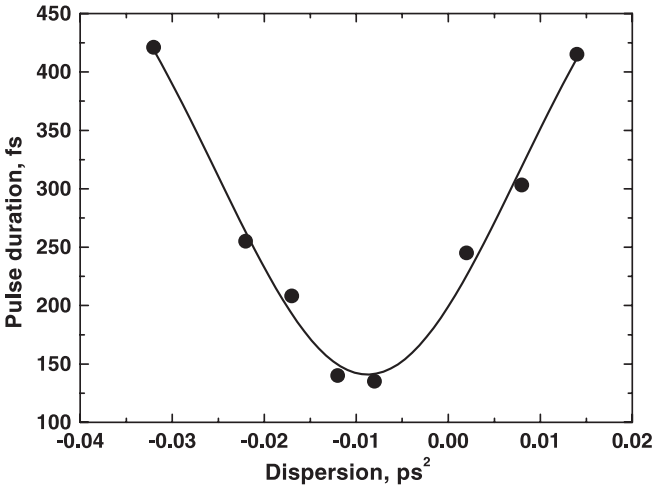

FIGURE 3 Pulse width versus external delay line dispersion for stretched-pulses with 22-nm bandwidth

A considerable amount of theoretical work has been done on mode locking with slow and fast saturable absorbers [8, 10, 11]. In particular, it has been shown that the presence of slow absorber has a remarkable impact on mode-locking stability. The impact of slow absorber becomes even more pronounced when the pulses have a large chirp, as in the case of stretched-pulse mode-locked lasers [11]. The operation guidelines derived from analysis of using fast and slow saturable absorbers for the mode locking of lasers allow for an optimal balance of two absorbers to achieve required power level, pulse duration and stability with a given laser system. The saturation fluence and absorber modulation depth are the most important parameters that control the start-up capability of the mode-locking process and pulse break-up [5]. The theoretical analysis shows that it is possible to vary the saturation fluence of the absorber by changing the device parameters [5]. Tighter focusing onto the SESAM reduces the absorber saturation energy. Another method of varying the saturation fluence involves changing the reflectivity of the top mirror. Finally, using a thinner absorber layer, i.e. changing the strength of the absorber, can change the non-linear modulation depth. In Sect. 3 we discuss some SESAM structure design guidelines for enhancing the non-linear response. With the two-absorbers configuration, these parameters for the saturable absorbers can be changed independently; therefore the contribution of each absorber to the mode locking process can be controlled. Eventually, the two-absorber set-up allows an increase in the stability range of given mode-locking regime.

3 Non-linear and dispersion properties of near-resonant saturable absorbers

3.1 *Non-linear reflectivity of anti-resonant and near-resonant SESAMs*

Low-absorption, anti-resonant devices are appropriate for lasers with low single-pass gain, such as solid-state lasers. To achieve large optical non-linearity, a near-resonant Fabry–Pérot geometry composed of a pair of asymmetric mirrors separated by a saturable absorber is used. This configuration provides a high on/off ratio by decreasing the reflection at low intensity. The highly non-linear response is needed for high-power pulse lasers; it is favorable for rapid self-starting of mode locking, particularly in a laser with large output coupling [12]. However, near-resonant SESAMs are not generally suitable for low-gain lasers because their losses are higher than the losses of anti-resonant SESAMs. The use of near-resonant SESAMs in erbium fiber lasers is appropriate because of their high gain.

Figure 4 shows the reflectivity of a typical near-resonant device measured as a function of the incident pulse energy. The absorber structure for this sample consisted of five groups of seven-period MQWs placed in a $5\lambda/2$ microcavity. The reflectivity from the top surface of the structure was approximately 30%. Since we exploit the microcavity effect to enhance the non-linear response, the on/off contrast ratio ΔR between the reflectance at high and low pulse energies depends on the wavelength detuning from the cavity resonance. Strong contrast improvement at $\lambda = 1558$ nm near the cavity resonant wavelength (~ 1570 nm) was observed, as can be seen in Fig. 4. The low-intensity spectrum of the device is shown in Fig. 5. For near-resonant operation, the non-linear reflectivity varied from 30 to 70%. Indeed, a much higher contrast ratio can be obtained for resonance operation at the expense of an increased insertion loss.

The non-linear response ΔR was also studied as a function of the volume of the absorbing MQW layer. Figure 6 shows the dependence of ΔR versus number of quantum wells within absorber layer. The non-linear response was significantly improved with an increase in the number of quantum wells for near-resonant operation. However, as the volume of the MQW layer increases, the switching energy will also increase.

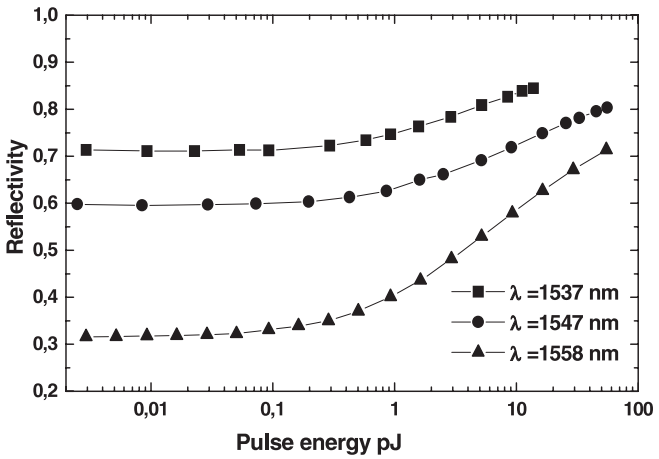

FIGURE 4 Non-linear reflectivity measurements as a function of the input energy for excitation with 600-fs-duration pulses

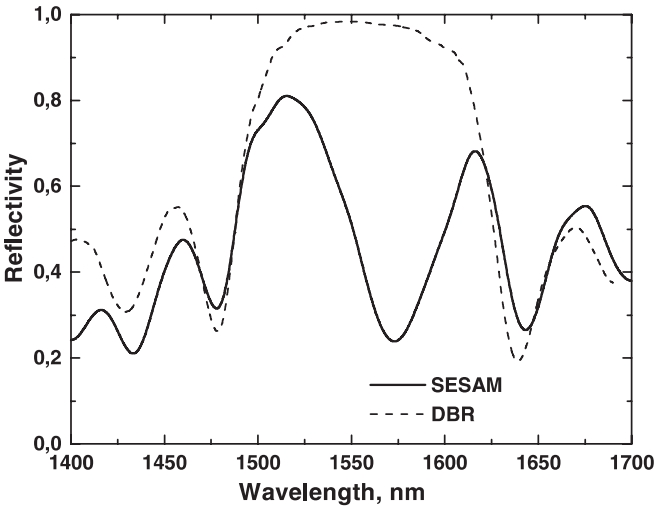

FIGURE 5 Low-intensity reflectivity of the near-resonant SESAM and the bottom mirror of the microcavity (DBR)

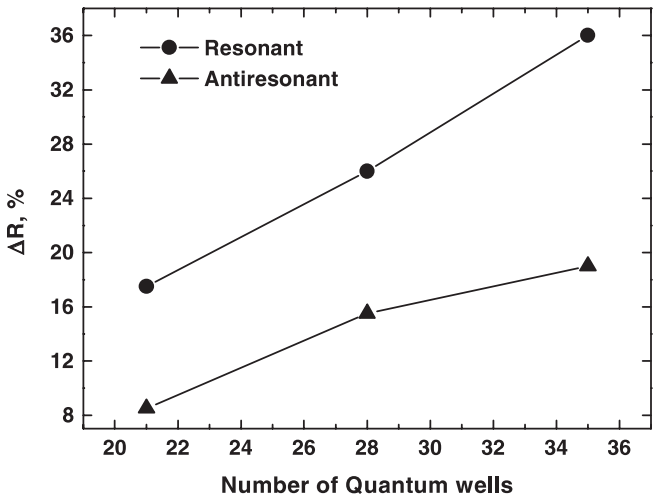

FIGURE 6 Contrast of non-linear reflectivity for near-resonant and anti-resonant conditions against number of quantum wells in the absorber layer

In addition, near-resonant SESAMs provide a convenient dispersion compensation technique, although have a trade-off in terms of bandwidth and tunability [13].

3.2 *Dispersion compensation by the D-SAM with negative GVD*

Ultrashort pulses can only be generated by the implementation of dispersion compensation in the laser cavity. Either bulk optic compensators or compensating fiber can accomplish dispersion management in the laser cavity. However, in all-fiber environmentally stable cavity designs, non-linear effects in the fiber eventually limit the maximum extractable power. Chirped mirrors are useful for the compression of high-energy pulses, since they produce high dispersion with negligible non-linear effects. Particularly attractive designs consist of a dispersive mirror structure in the form of a Gires–Tournois interferometer (GTI) that includes the semiconductor saturable absorber. These structures are simple to

fabricate and integrate into the laser cavity and can produce large amounts of both negative and positive dispersion. Controllable dispersion may be achieved using GTI-based saturable absorber mirrors, i.e. dispersive saturable absorber mirrors (D-SAMs), thus allowing chirp-free pulse or high-power stretched-pulse lasers to be realized. The trade-off in terms of the amount of induced dispersion, optical bandwidth and tunability can be reached by optimization of the free spectral range and finesse of the GTI. By exploiting the dependence of the Fabry–Perot reflection response on the laser beam focusing, or by tuning the operation wavelength, we can adjust the amount of dispersion introduced by D-SAM.

In a stretched-pulse laser, the output pulses have a large positive chirp, which can then be compressed with an external dispersive delay line of negative dispersion fiber [3]. However, non-linear effects in the fiber dispersive delay line limit the maximum output power in this technique. Chirp compensation using prism- or grating-based compensators has allowed external and intracavity pulse compression, but adds more complexity to the laser system [3, 14]. Recently, a dispersion-compensating saturable absorber mirror based on a semiconductor Gires–Tournois-like Fabry–Perot structure was used for intracavity dispersion compensation [13]. The D-SAM operated close to the Fabry–Perot resonance, combining both saturable absorption and negative (or positive) GVD in one element. The D-SAM was used in a stretched-pulse mode-locked fiber laser as a saturable absorber and intracavity dispersion compensator. By controlling the amount of negative dispersion introduced by the D-SAM, we were able to generate high-power chirp-free pulses directly from a stretched-pulse laser.

The experimental set-up for the stretched-pulse mode-locked laser is similar to the one shown in Fig. 1, except for the fast absorber, which was replaced by a broadband dielectric mirror and the slow absorber, which was replaced by the D-SAM. The saturable absorber region consisted of six 6-nm-thick $Ga_{0.245}In_{0.755}As_{0.7}P_{0.3}$ quantum wells separated by 20-nm-thick $Ga_{0.245}In_{0.755}As_{0.49}P_{0.51}$ barriers, grown by molecular beam epitaxy. For D-SAM, we used a low-finesse Fabry–Perot gold-based design similar to the one described in [15], where the top reflector is formed by the 27% Fresnel reflection of the semiconductor/air interface and gold film is deposited as the bottom reflector. To improve the reflectivity of the metal-coated structure, we inserted a SiO_2 layer between the metal and the semiconductor. Finally, the D-SAM was glued onto a glass substrate. The free spectral range of the Fabry–Perot, mainly determined by the thickness of the InP spacer layer, was approximately 16.5 nm. The thickness of the Fabry–Perot cavity was adjusted to achieve a resonant wavelength close to 1552 nm. Depending on the operation regime, the focal spot size on the saturable absorber was varied in the range 5–10 μm. The average GVD of the fiber section of the cavity was $+0.029\,ps^2$ in the normal dispersion regime. The low-power reflectivity of the D-SAM was measured in situ for each focusing lens adjustment corresponding to each operation regime.

The low-intensity reflectivity and calculated group delay [15] of the absorber mirror operated at anti-resonance is shown in Fig. 7a. As shown in Fig. 7b, the pulse spectrum

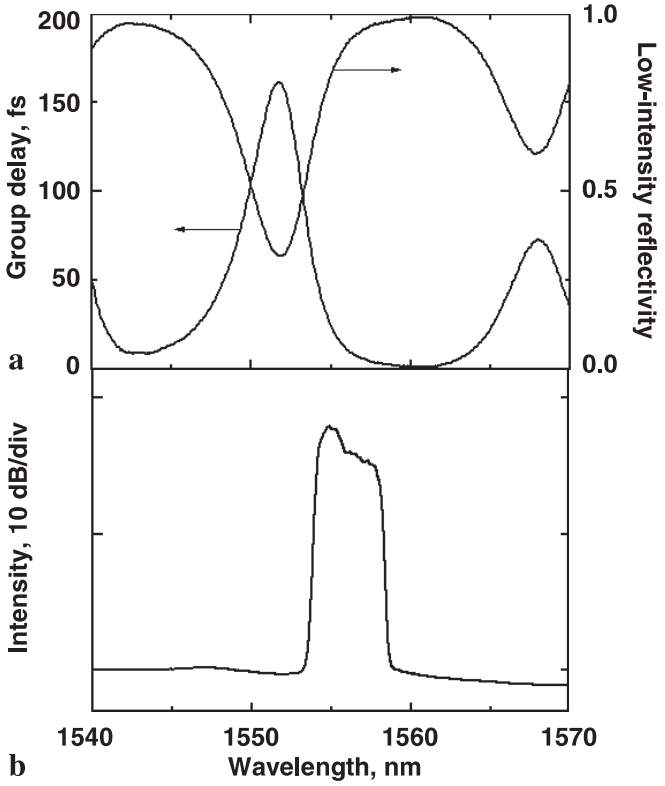

FIGURE 7 **a** Measured reflectivity and the calculated group delay of the absorber mirror adjusted for anti-resonance; and **b** the pulse spectrum

had a square shape, supporting the formation of a chirped-pulse structure. It can be seen that within the pulse spectral bandwidth of $\Delta\lambda = 4$ nm, the group delay dispersion of the absorber mirror is low, therefore forcing the laser to operate in the stretched-pulse regime. Corresponding autocorrelation of the positively chirped pulse is shown in Fig. 8. The maximum average output power of the laser was 30 mW. However, the pulse breaks up into multiple pulses with increasing in pump power, thus limiting the pulse energy to approximately 0.5 nJ. Producing multi-nJ pulses would be possible by suppressing

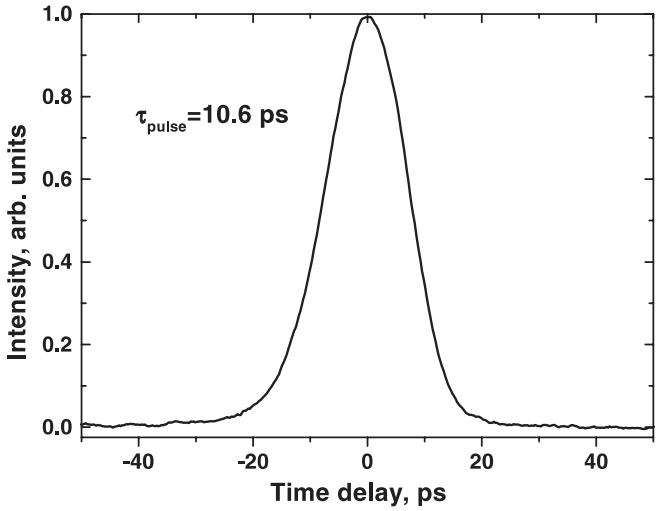

FIGURE 8 Autocorrelation of the pulse using an anti-resonant saturable absorber regime

the multiple-pulse break-up, e.g. by using fast and slow absorbers as cavity mirrors.

In order to run the laser in the negative GVD regime near Fabry–Perot resonance and achieve pulse compression, we exploited the dependence of Fabry–Perot reflectivity on laser beam focusing [15]. It has been shown that this effect could be used to force near-resonant operation of a saturable absorber. The reflectivity of the D-SAM, modified by minor changes in the focusing condition, controls the wavelength of the mode-locked pulses. This approach resulted in a laser design which is simple and easy to align, as no intracavity prisms or gratings have to be used.

The measured reflectivity and calculated group delay of the D-SAM, with lens focusing corresponding to near-resonant operation with negative GVD near $\lambda = 1553$ nm are shown in Fig. 9a. As can be seen, the positive slope of group delay, corresponding to negative GVD, is close in the wavelength domain to the reflection maximum of the D-SAM. This result suggests that laser operation will be possible in the negative GVD regime. Indeed, a 2.3-nm-wide pulse spectrum, trapped by the local reflection maximum of the D-SAM with negative dispersion, was observed, as shown in Fig. 9b. However, there is price to pay; the D-SAM reflectivity was decreased by approximately 15%–20%. In Fig. 10 we plot the corresponding autocorrelation of the 1.12-ps pulses, with a time–bandwidth product of 0.32, generated using chirp compensation by the D-SAM.

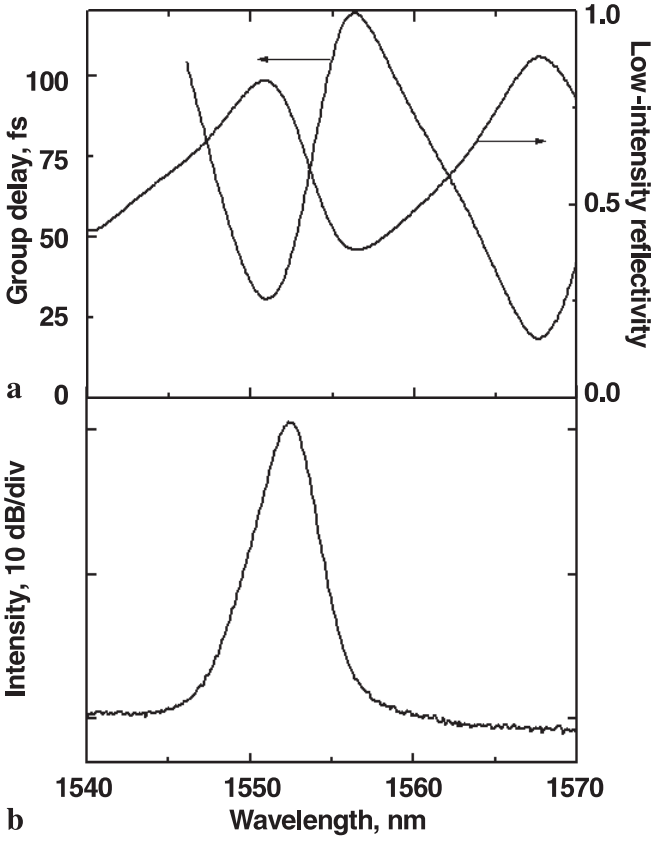

FIGURE 9 **a** Measured reflectivity and the calculated group delay of the D-SAM operated in the negative GVD regime; and **b** spectrum of pulses de-chirped by the intracavity D-SAM

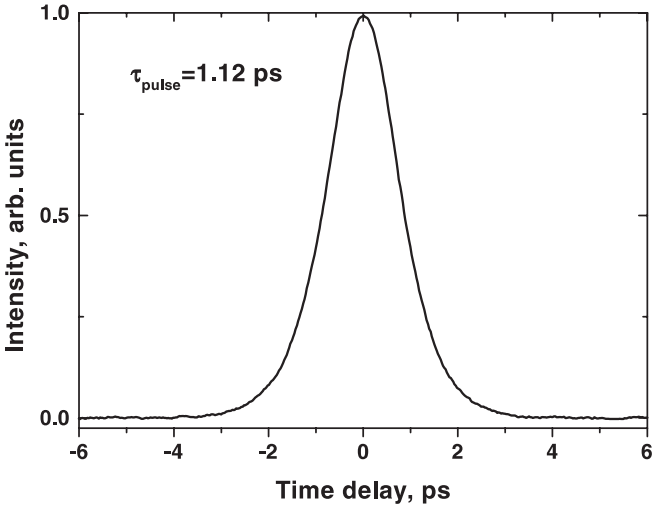

FIGURE 10 Autocorrelation trace of pulse from the stretched-pulse laser with D-SAM supporting negative GVD

3.3 *Pulse stretching by D-SAM with positive GVD*

In order to study the operation of the D-SAM with positive GVD, the average dispersion of the fiber segment of the cavity was changed to support the anomalous dispersion regime. The experimental set-up shown in Fig. 11, is similar to that described in Fig. 1, except for the dispersion-compensating fiber, which was removed, leading to a round-trip cavity dispersion of -0.05 ps^2 in the anomalous dispersion regime. Initially, in an attempt to increase the amount of D-SAM dispersion, we used a low-bandwidth D-SAM with a free spectral range (FSR) of approximately 20 nm. The spectral dependencies of the low-intensity reflectivity and group delay of the D-SAM are shown in Fig. 12a. A 10-nm tunable filter was used to define the operating wavelength. The effect of wavelength tuning is shown in Fig. 12b, which plots the pulse spectra for compressed and stretched pulse regimes. With 75 mW of pump power, the average output power was 3.7 dBm and 10.2 dBm, respectively, demonstrating the improvement in the pulse energy extraction for stretched-pulse operation. Corresponding autocorrelations are shown in Fig. 13, with a temporal stretching/compression factor of approximately 7.

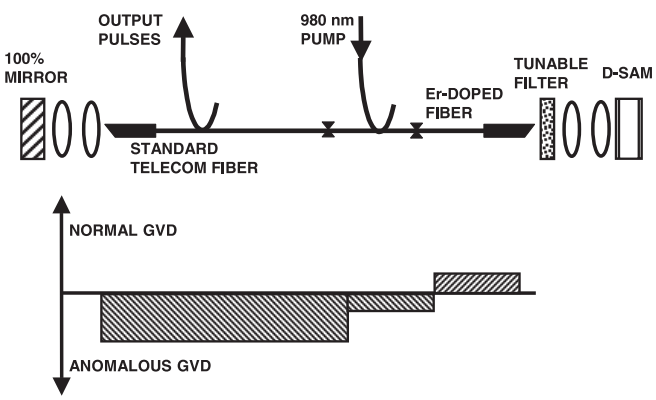

FIGURE 11 Set-up of the fiber laser with D-SAM and dispersion map of the cavity

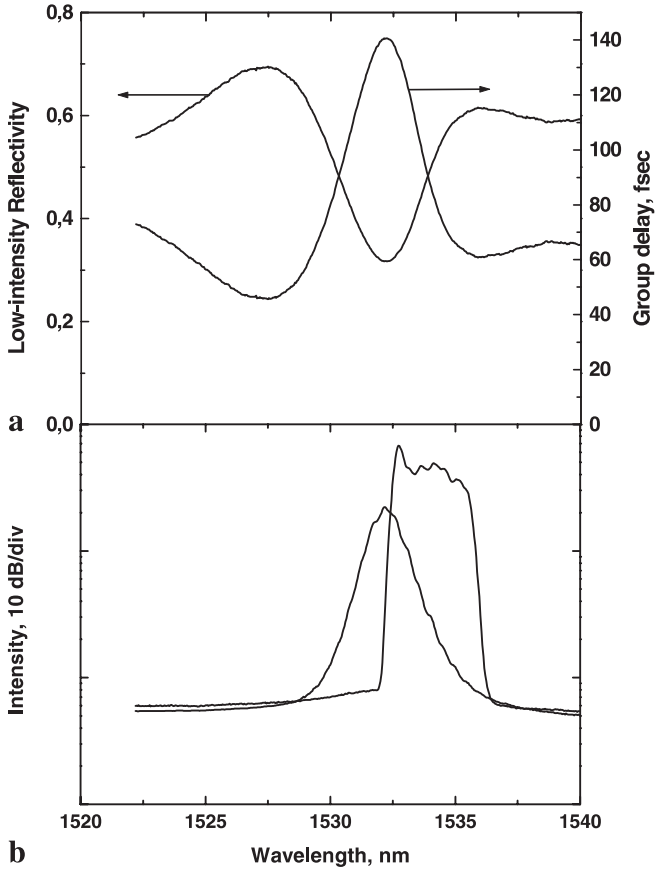

FIGURE 12 **a** Measured reflectivity and the calculated group delay of the D-SAM operated in the positive GVD regime; and **b** pulse spectrum for operation in the soliton regime and stretched-pulse regime

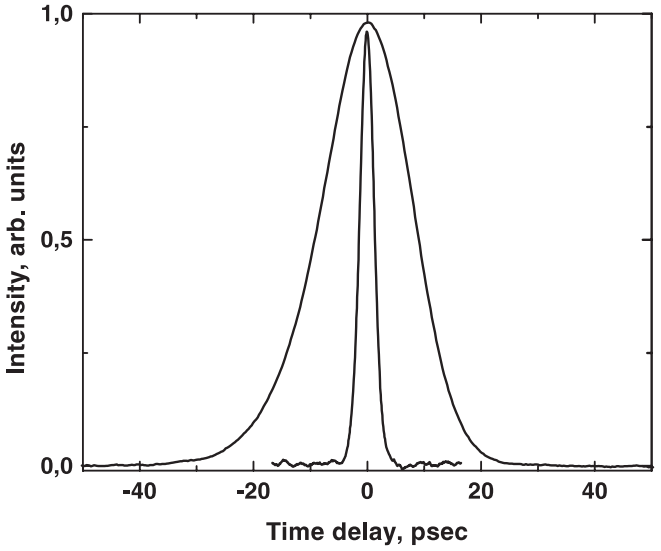

FIGURE 13 Autocorrelation traces for the operation in the soliton regime and stretched-pulse regime

To obtain a broadband operation, the FSR of the D-SAM has been increased to > 150 nm by decreasing the thickness of the spacer layer. The spectra of low-intensity reflectivity and group delay of the D-SAM are shown in Fig. 14. To compensate for the dispersion of the fiber cavity, the Fabry–Perot structure of the D-SAM was designed for positive (normal) GVD over the emission spectrum of the gain medium, i.e. 1525–1560 nm for the Er-doped fiber amplifier band. Figure 15 shows the non-linear reflectivity of the D-SAM measured as a function of the incident pulse energy

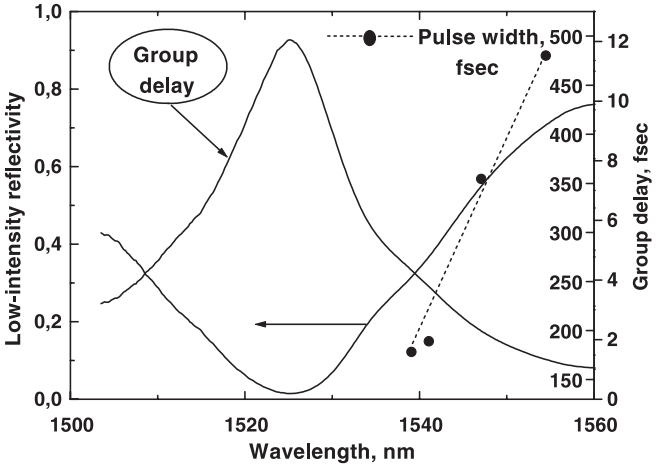

FIGURE 14 Low-intensity reflectivity and group delay of a D-SAM with positive GVD

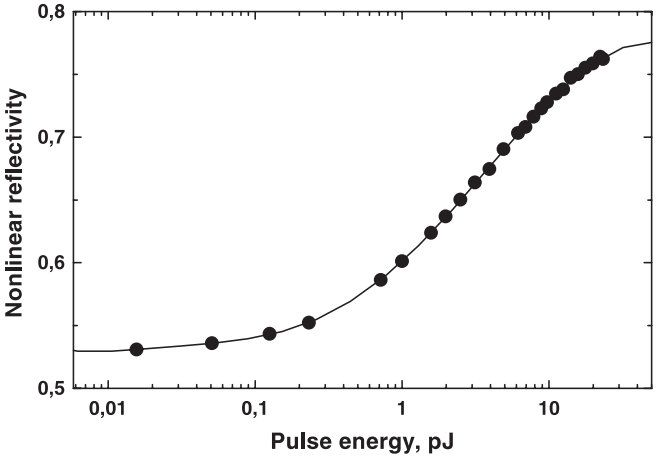

FIGURE 15 Non-linear reflectivity of the D-SAM operating near resonance

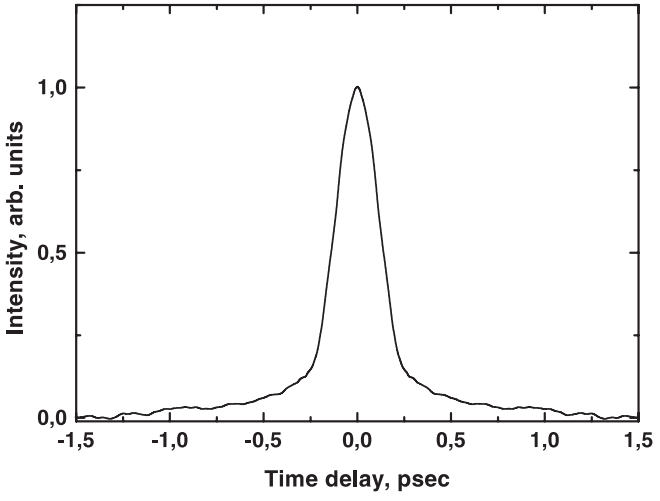

FIGURE 16 Autocorrelation trace for the pulses with minimum width owing to dispersion compensation provided by the D-SAM

at $\lambda \approx 1545$ nm. The high on/off contrast ratio between the low-intensity reflectivity and the reflectivity at 10 pJ pulse energy, i.e. non-linear modulation, was found, as seen in Fig. 15. While the laser was mode locked, the operation wavelength could be continuously tuned from 1560 nm to 1540 nm. As can be seen from Fig. 14, tuning to the shorter wavelength corresponds to an increase in the amount of positive dispersion induced by the D-SAM (negative slope of group delay corresponds to positive GVD), thus providing the compensation for the anomalous dispersion of the fiber section of the cavity. The shortest pulse width of 175 fs occurred for $\lambda \approx 1540$ nm. The compressed pulse autocorrelation is shown in Fig. 16.

4 Conclusions

In summary, we have demonstrated a novel stretched-pulse fiber laser using slow and fast semiconductor saturable absorbers. We can independently optimize the operation of slow and fast absorbers so that the laser self-starts reliably without multiple pulse break-up, generating 1.3 nJ background-free fundamental pulses. We have shown that the dispersion of a D-SAM can significantly affect the mode-locking behavior. The trade-off in terms of the amount of induced dispersion, optical bandwidth and tunability can be reached by optimization of the free spectral range and finesse of the D-SAM. Dispersion tuning obtained with D-SAM allows direct comparison of pulse energy extraction in the soliton-supporting dispersion regime and in the stretched-pulse mode-locking regime. By changing the operation regime, accomplished by wavelength tuning, it has been confirmed that the extractable pulse energy in a soliton fiber laser can be increased significantly by chirping the pulses inside the laser cavity. We have shown that D-SAMs can be optimized to produce tailored dispersion characteristics over bandwidths of tens of nanometers.

ACKNOWLEDGEMENTS The authors thank T. Sajavaara for the heavy ion implantation and A. Vainionpää, S. Suomalainen and J. Lyytikäinen for the assistance with MBE growth. This research was supported by the Finnish Academy of Science (RHINO project) and Technology Development Center of Finland (ULTIMA project).

REFERENCES

1 D.J. Jones, L.E. Nelson, H.A. Haus, E.P. Ippen: IEEE J. Sel. Top. Quant. Electron. **3**, 1076 (1997)
2 L.E. Nelson, D.J. Jones, K. Tamura, H.A. Haus, E.P. Ippen: Appl. Phys. B **65**, 277 (1997)
3 L.E. Nelson, S.B. Fleischer, G. Lenz, E.P. Ippen: Opt. Lett. **21**, 1759 (1996)
4 C.R. Doerr, H.A. Haus, E.P. Ippen, M. Shirasaki, K. Tamura: Opt. Lett. **19**, 31 (1994)
5 F.X. Kärtner, J. Aus der Au, U. Keller: IEEE J. Sel. Top. Quant. Electron. **4**, 159 (1998)
6 N. Xiang, O. Okhotnikov, A. Vainionpää, M. Guina, M. Pessa: Electron. Lett. **37**, 374 (2001)
7 E. Lugagne Delpon, J.L. Oudar, N. Bouché, R. Raj, A. Shen, N. Stelmakh, J.M. Lourtioz: Appl. Phys. Lett. **72**, 759 (1998)
8 U. Keller, D.A.B. Miller, G.D. Boyd, T.H. Chiu, J.F. Ferguson, M.T. Asom: Opt. Lett. **17**, 505 (1992)
9 D. von der Linde: Appl. Phys. B **39**, 201 (1986)
10 H.A. Haus: IEEE J. Quant. Electron. **QE-3**, 169 (1976)
11 J.C. Chen, H.A. Haus, E.P. Ippen: IEEE J. Quant. Electron. **29**, 1228 (1992)
12 M. Jiang, G. Sucha, M.E. Fermann, J. Jimenez, D. Harter, M. Dagenais, S. Fox, Y. Hu: Opt. Lett. **24**, 1074 (1997)
13 D. Kopf, G. Zhang, R. Fluck, M. Moser, U. Keller: Opt. Lett. **21**, 486 (1996)
14 J.H.V. Price, L. Lefort, D.J. Richardson, G.J. Spühler, R. Paschotta, U. Keller, C. Barty, A. Fry, J. Weston: In: Conf. on Lasers and Electro-Optics, Vol. 56, 2001, OSA Trends in Optics and Photonics Series, p. 219 (2001)
15 O.G. Okhotnikov, M. Guina: Opt. Lett. **25**, 1624 (2000)
16 M. Beck, I.A. Walmsley, J.D. Kafka: IEEE J. Quant. Electron. **27**, 2074 (1991)